HHS Public Access

Author manuscript

J Neural Eng. Author manuscript; available in PMC 2018 December 09.

Published in final edited form as:

J Neural Eng. 2018 December ; 15(6): 066003. doi:10.1088/1741-2552/aadb49.

A novel re-attachable stereotactic frame for MRI-guided neuronavigation and its validation in a large animal and human cadaver model

Christine A. Edwards[1,2,3], **Aaron E. Rusheen**[2,4], **Yoonbae Oh**[2], **Seungleal B. Paek**[2,3], **Joshua Jacobs**[2], **Kristen H. Lee**[2], **Kendall D. Dennis**[5], **Kevin E. Bennet**[2,5], **Abbas Z. Kouzani**[1], **Kendall H. Lee**[2,3,4,6,7], and **Stephan J. Goerss**[2]

[1]School of Engineering, Deakin University, Geelong, VIC 3216, Australia

[2]Department of Neurologic Surgery, Mayo Clinic, Rochester, MN, United States of America

[3]Mayo Clinic Graduate School of Biomedical Sciences, Mayo Clinic, Rochester, MN 55905, United States of America

[4]Mayo Clinic School of Medicine, Mayo Clinic, Rochester, MN 55905, United States of America

[5]Division of Engineering, Mayo Clinic, Rochester, MN 55905, United States of America

[6]Department of Physiology and Biomedical Engineering, Mayo Clinic, Rochester, MN, United States of America

Abstract

Objective.—Stereotactic frame systems are the gold-standard for stereotactic surgeries, such as implantation of deep brain stimulation (DBS) devices for treatment of medically resistant neurologic and psychiatric disorders. However, frame-based systems require that the patient is awake with a stereotactic frame affixed to their head for the duration of the surgical planning and implantation of the DBS electrodes. While frameless systems are increasingly available, a reusable re-attachable frame system provides unique benefits. As such, we created a novel reusable MRI-compatible stereotactic frame system that maintains clinical accuracy through the detachment and reattachment of its stereotactic devices used for MRI-guided neuronavigation.

Approach.—We designed a reusable arc-centered frame system that includes MRI-compatible anchoring skull screws for detachment and re-attachment of its stereotactic devices. We validated the stability and accuracy of our system through phantom, *in vivo* mock-human porcine DBS-model and human cadaver testing.

Main results.—Phantom testing achieved a root mean square error (RMSE) of 0.94 ± 0.23 mm between the ground truth and the frame-targeted coordinates; and achieved an RMSE of 1.11 ± 0.40 mm and 1.33 ± 0.38 mm between the ground truth and the CT- and MRI-targeted coordinates, respectively. *In vivo* and cadaver testing achieved a combined 3D Euclidean localization error of 1.85 ± 0.36 mm ($p < 0.03$) between the pre-operative MRI-guided placement and the post-operative CT-guided confirmation of the DBS electrode.

[7] Author to whom any correspondence should be addressed. lee.kendall@mayo.edu (K H Lee).

Significance.—Our system demonstrated consistent clinical accuracy that is comparable to conventional frame and frameless stereotactic systems. Our frame system is the first to demonstrate accurate relocation of stereotactic frame devices during *in vivo* MRI-guided DBS surgical procedures. As such, this reusable and re-attachable MRI-compatible system is expected to enable more complex, chronic neuromodulation experiments, and lead to a clinically available re-attachable frame that is expected to decrease patient discomfort and costs of DBS surgery002E

Keywords

stereotactic surgery; stereotactic frame; neuronavigation; deep brain stimulation

Introduction

In this modern era of functional neurosurgery, stereotactic technologies are ubiquitous and a necessity to safely and accurately access deep brain regions for diagnosis and treatment of a myriad of neurologic disorders and pathologies. The foundations of modern-day stereotactic systems date back nearly a century when Horsley and Clarke developed the first stereotactic device to navigate to deep brain structures for animal experiments (Picard *et al* 1983). Coupling stereotactic techniques with innovative brain imaging methods enabled the translation of these technologies for clinical use. As such, mid-twentieth century pioneers of stereotactic neurosurgery, Spiegel and Wycis, demonstrated the first human stereotactic system (Spiegel *et al* 1947). It leveraged pneumoencephalography for localization of intracranial patient-specific landmarks to precisely identify stereotactic coordinates used to lesion specific subcortical nuclei. This was followed by the publication of their foundational comprehensive collection of stereotactic atlases of the human brain (Spiegel and Wycis 1952). Breakthrough advances in neuroimaging technologies—computed tomography (CT) in the 1970s and magnetic resonance imaging (MRI) in the 1980s—enabled safer visualization of more reliable anatomical landmarks, such as the anterior and posterior commissure points. Today, localization of these reference points remains standard practice to align patient-specific image volumes to stereotactic atlases, and enables estimation of the location of other intracranial structures for stereotactic surgery planning and neuronavigation.

An important application of MRI-guided stereotactic functional neurosurgery is deep brain stimulation (DBS) therapy. To date, over 100 000 patients worldwide are implanted with DBS systems that are providing therapeutic relief from debilitating treatment-resistant neurologic and psychiatric disorders (Shen 2014). However, the surgical procedure itself has remained relatively unchanged since its inception over thirty years ago (Benabid *et al* 1987, Sironi 2011). Although the surgical procedure varies from institution to institution, its success depends on the accurate placement of DBS electrodes into targeted brain structures, supported by precision stereotactic devices (Nakazawa *et al* 2014, Neumann *et al* 2015, Seibert *et al* 2016). The gold-standard traditional stereotactic system- the Leksell™ (Elekta, Stockholm, Sweden)- achieves this precision through a rigid head frame that remains affixed throughout the surgical planning and electrode placement to preserve the precision of the stereotactic coordinate space as mapped to the patient's anatomy through MR images. A limitation of such a system however, is the discomfort of the head frame and the need to

perform neuroimaging, surgical planning, and implantation all in a single day. While local anesthesia is administered to reduce such discomfort, many patients still experience increased pain from the insertion pins used to secure the frame to the skull and which penetrate the scalp and remain in-place throughout the procedure (Wang *et al* 2014). Furthermore, the weight of the frame apparatus and the requirement for the patient's head to remain in a fixed position throughout the procedure contribute to its discomfort. Thus, a stereotactic frame system that is re-attachable is desirable to enable the separation of planning and implantation stages of the DBS surgical procedure, which in turn may reduce the duration of the procedure and improve patient comfort.

Previously, we developed computer-assisted stereotactic devices for both clinical (Kelly *et al* 1987) and basic research applications, including the first version of an MRI-compatible porcine stereotactic head frame combined with a Leksell™ arc quadrant (Knight *et al* 2013), a nonhuman primate (NHP) stereotactic system (Min *et al* 2014), and an MRI-compatible spine stereotactic system (Grahn *et al* 2016). Herein, we describe the design, development, fabrication and preclinical testing of our novel re-attachable stereotactic head frame system for DBS neurosurgery that is reusable and high-field MRI-compatible.

Materials and methods

MRI-compatible stereotactic system design & development

The design of our re-attachable stereotactic frame system was performed with the aid of SolidWorks® (Dassault Systèmes, Vélizy-Villacoublay, France), and the frame system was fabricated in-house. Our mock-human porcine system includes novel MRI-compatible skull anchor screws composed of polyetheretherketone (PEEK), a surgical template to implant the screws (figure 1(A)), an MRI-compatible acrylic stereotactic localization system (figure 1(B)) and an arc-centered head frame system (figure 1(C)). The localization and head frame systems were designed to be re-attachable to the skull anchor screws, while maintaining the stability and accuracy of the stereotactic space for neuronavigation. Furthermore, our system was designed to be compatible with existing computer-assisted surgical planning software (i.e. COMPASS™, COMPASS International Innovations, Rochester, MN, USA) used to identify the trajectory path of the electrode to the DBS target and provide stereotactic space coordinates used for the surgical procedure (Min *et al* 2012).

Image-guided stereotactic surgery planning software requires visible fiducial markers within MR or CT image volumes to align and register the images to stereotactic space. These fiducial markers are created using an N-bar localizer box. We designed an MRI-compatible porcine localizer box with N-shaped grooves in bilateral vertical planes and a superior horizontal plane suspended around the head (figure 1(B)). For MR imaging, the N-shaped grooves were fitted with flexible tubing that is filled with a 2.0% copper sulfate solution; for CT imaging, the N-shaped grooves were fitted with aluminum vertical bars. In both cases, image cross-sections of the diagonal and vertical bars of the N-shaped elements appear as ellipsoid and circular artifacts respectively, that function as the fiducials. The fiducials are needed to calculate the location of each image in stereotactic space and create an image volume aligned with the stereotactic coordinate system (Goerss *et al* 1982). The registered

image volume is used by stereotactic surgerical planning software to determine stereotactic target and trajectory coordinates.

Like other common stereotactic frame systems, such as the Leksell™ (Elekta Instruments, Tucker, GA, USA), the Cosman–Roberts–Wells (Radionics®, Burlington, MA, USA), and the COMPASS™ system, (COMPASS International Innovations, Rochester, MN) our frame system was designed based on the arc-quadrant principle. With this design, the probe is held along the normal vector of the 160 mm radius arc quadrant, projecting a path through the center of the arc quadrant, called the focus. The radius determines the depth to the stereotactic target, located at the focus. The two degrees of freedom of the arc-quadrant, the arc and collar angles, are manipulated to approach the focus in a myriad of directions. Linear adjustments made with the 3D slide (X, Y, and Z) move the arc-quadrant left/right, caudal/rostral, and dorsal/ventral to bring the focus to the surgical target. The output of planning software provides the values of the target coordinates (X_T, Y_T, Z_T) and the surgical trajectory (Collar and Arc angles). Duplicating these values on the stereotactic device emulates the surgical plan.

The overall stability and accuracy of our re-attachable stereotactic frame system was validated through phantom, *in vivo* pig, and human cadaver testing. Phantom tests were conducted to quantify the mechanical accuracy of the stereotactic frame system to target phantom test points. Furthermore, our MR and CT stereotactic localization systems were attached to the phantom, and stereotactic surgerical planning software was used to target each phantom point within the MR and CT image volumes. For each test, the 3D distance between the physical coordinates and targeted coordinates of each phantom point was calculated, and the root mean square error was determined. *In vivo* pig and human cadaver tests were conducted to assess the biomechanical stability of the skull anchor screws and to evaluate the stereotactic system accuracy in the context of implanting a DBS electrode. The experimental design emulated a clinical DBS technique: a preoperative MRI to determine the stereotactic target and trajectory coordinates to implant the electrode, and a postoperative CT to confirm proper placement of the DBS lead. The overall stereotactic system accuracy was evaluated by determining the 3D distance between the desired target location and the position of the DBS lead as determined by the postoperative CT scan.

Repeatability and accuracy validation: phantom testing

A customized MRI-compatible phantom was designed and fabricated in-house to evaluate the accuracy and repeatability of our re-attachable stereotactic frame system. The test phantom includes nine pointed cylindrical acrylic targets, which reside in the work envelope of our stereotactic system when attached to the base of the head frame (figure 3(A)). The physical coordinates of the phantom test points were based on the mechanical design created in SolidWorks® and verified by the machinist. As such, these known spatial coordinates are considered the ground truth and were used for comparison to validate the accuracy of the system. To assess the mechanical accuracy of the stereotactic frame system, a probe positioned at the focus of the arc-quadrant system was adjusted to touch the tip of each phantom target. The X, Y, and Z coordinates of the stereotactic frame system were recorded for all nine phantom target points (figure 3(B)). The process of targeting all nine phantom

points was repeated three times, with the frame removed and then reattached prior to each set of measurements. To further demonstrate repeatability, three independent users conducted this mechanical accuracy test and their measurements were compared with the known spatial coordinates of the phantom points. The 3D distance between the known physical coordinates of the phantom and the stereotactic frame coordinates were calculated. To assess image error in a controlled setting, MR and CT image volumes of the phantom were acquired with the customized N-bar localizer box mounted to it (figures 3(C)–(E)). Stereotactic surgery planning software (i.e. COMPASS™) was used to calculate the image coordinates of each phantom point in the stereotactic space.

Stability and accuracy validation: in vivo testing

A mock-human porcine MRI-guided DBS surgical procedure using the described re-attachable stereotactic frame system was developed and performed in accordance with the National Institutes of Health Guidelines for Animal Research and the Mayo Clinic Institutional Animal Care and Use Committee. The subject group consisted of five normal domestic male pigs, weighing 30 ± 5 kg, with the ventral tegmental area (VTA) chosen as the DBS target for proof of principle (Settell *et al* 2017). Each subject was intubated, and sedation was maintained with isoflurane (1%–3%) throughout the surgical procedure. The MRI-guided surgical approach was much like previously described clinical (Edwards *et al* 2017) and animal (Knight *et al* 2013) DBS procedures that used frame-based stereotactic systems. However, our stereotactic frame system differed by requiring precise orientation and spacing of skull anchor screws to preserve the spatial accuracy of the stereotactic system throughout the procedure. As such, we developed and validated a surgical method to implant the skull anchor screws. Following the implantation of the skull screws, MRI-based targeting was performed to determine the stereotactic coordinates of the DBS target (X, Y, Z) and trajectory (collar, arc). The DBS electrode was implanted unilaterally to the target, and a postoperative CT scan was acquired to confirm the electrode placement.

Implanting skull anchor screws.

First, the anchor screw template (figure 1(A)) was centered over the skull and slight pressure was applied to mark the scalp with four sharp indexing pins located on the bottom side of the template adjacent to each screw opening. Next, a 1.0 cm scalp incision was made to the surface of the skull at each of the marked sites. The template was repositioned onto the skull with the sharp indexing pins passing through each incision. After which a band was tied around the template and jaw to securely hold the template in-place while the following steps were performed to implant each skull anchor screw: (1) removed the sharp indexing pin from the drill guide, (2) inserted a 5.1 mm drill bit with a fixed depth into the drill guide to create a hole of a fixed depth in the skull, (3) replaced the drill guide with a driver and anchor screw assembly (figure 1(A)) to implant the self-tapping skull anchor screw into the twist drill hole, and (4) rotated the cam clamp to fix the driver into position. After completing Steps 1–4 to implant each screw, the skull anchor screws were released from the anchor driver assembly, the skull anchor drivers were removed from the template, and the template was lifted off of the skull anchor screws, which left the anchor screws in a precise pattern securely implanted in the skull. Upon completion, the top surface of each anchor screw flange resided on a single plane, defining the reference plane needed to align image

space (the attachment of the image localizer) to physical space (the attachment of the stereotactic head frame).

MRI acquisition and target planning.

First, guide rods screwed into the skull screws were used to position an inhouse custom MRI four-channel phased array radio frequency coil (Mayo Clinic, Rochester, MN, USA) on the surface of the head. This coil enhances the signal to noise ratio as previously demonstrated for large animal 3.0 T functional MRI studies (Min *et al* 2012). Next, the guide rods were used to position the image localization bracket above the coil and onto the anchor screws where it was secured with Delrin™ thumbscrews. The MRI N-bar localizer box was attached to the localization bracket with nylon screws. Once the MRI-compatible localization system was secured to the skull anchor screws, with the N-bar localizer suspended about the subject's head, the subject was positioned in a 3.0 Tesla MR scanner (Signa™ HDx, General Electric, Wakasha, WI, USA). An anatomical image volume was acquired using the MRI protocol based upon prior mock-human porcine DBS studies, which lever-aged the commonly used 3D magnetization prepared rapid gradient-echo (MP-RAGE) sequence to acquire coronal high-resolution 3D structural brain images with a slice thickness of 0.8 mm and field of view of 24 × 24 cm. The field of view region was adjusted to ensure the N-bar localizer fiducials were visible in the MR images. Upon completion of the MRI scan, the N-bar localizer, bracket and head coil were removed and the images were transferred to the surgical planning computer. A DBS surgical plan comprised of the electrode stereotactic target coordinates and an optimal trajectory was created using a previously modified version of COMPASS™ navigational software used for large animal studies (Knight *et al* 2013). The anterior commissure–posterior commissure line was manually identified in the anatomical MRI data, and COMPASS™ software was used to co-register the image data to a stereotactic pig atlas (Felix *et al* 1999). The software was then used to plan a DBS electrode target and trajectory to the VTA, resulting in the stereotactic target coordinates (X, Y, Z) and the trajectory settings (collar, arc) needed to implant the electrode.

DBS electrode implantation.

The base of the stereotactic head frame system was attached to the four skull anchor screws. The settings for the stereotactic device were adjusted to match the DBS target coordinates and the arc and collar angle values derived during the surgical planning process. For electrode delivery, a NeuroNav Drive™ (Alpha Omega Co., Alphraretta, GA, USA) and cannula holder were secured to the arc. The stereotactic arc quadrant system was then attached to the base of the head frame. The DBS lead insertion cannula was inserted into the instrument carrier and advanced to the scalp to mark the entry site of the electrode. Next, a 5–10 mm burr hole was created, which was centered about the planned entry site. The stereotactic arc quadrant settings and the DBS target coordinates values were confirmed prior to inserting the delivery cannula into the brain. The delivery cannula was of a fixed length matching the radius of the arc, placing the distal end of the cannula at the focus. The DBS electrode was inserted into the delivery cannula and advanced to the focus using the NeuroNav Drive™. A Medtronic Model 3389 DBS electrode (containing four contacts that are 1.27 mm in diameter, 1.5 mm in length, and spaced 0.5 mm apart) was used for the first

two *in vivo* experiments; and a NuMed (NuMed, Inc., Hopkinton, NY, USA) DBS electrode (containing six contacts that are 0.625 mm in diameter, 0.5 mm in length, and spaced 0.5 mm apart) was used for the remaining *in vivo* and cadaver experiments. Once the DBS lead was in position, the delivery cannula was withdrawn until the DBS lead, still being held by the microdrive, was visible. Next the lead was secured to the skull using either UV cured epoxy, a titanium microplate, or a Stimloc™ (Medtronic, Minneapolis, MN, USA). Once secured, the stereotactic frame was removed, leaving the skull anchor screws in-place to acquire a post-operative CT scan.

CT acquisition and electrode confirmation.

The CT localization system bracket was secured to the four skull anchor screws, and the N-bar localizer was attached to the bracket. Once the N-bar localizer was secured, the subject was positioned in a CT (Dual source Somatom Definition, Siemens AG) scanner to acquire a postoperative anatomical image volume to confirm the placement of the electrode using COMPASS™ software. The CT N-bar localizer fiducials were manually identified to reconstruct the postoperative stereotactic space and then aligned to the stereotactic pig atlas (Felix *et al* 1999). MRI-guided preoperative DBS electrode trajectory to target was overlaid onto the CT images, and the corresponding stereotactic coordinates of the implanted electrode were determined. In addition, 3D Slicer (Fedorov *et al* 2012) software was used to align the post-operative CT images to the preoperative MRI images to further assess the distance of the electrode from the intended target.

Stability and accuracy validation: cadaver testing

The MRI-guided DBS surgical procedure was performed on a human cadaver head, similar to that of our porcine experiments. To accommodate for the increased cranial bone curvature of the human skull at the location of the stereotactic frame placement, adjustments were made to the system design. This entailed creating an enlarged DuPont™ Delrin® base frame with custom screw anchor brackets positioned at a 45° angle, which were used both to guide the implantation of the screws and as an adapter to attach the stereotactic device.

Implanting skull anchor screws.

The modified skull anchor screw template was centered over the skull to position the two anterior skull anchor screws approximately 8 cm superiorly from the supraorbital notch. Based on the skull anchor template, incision points at each screw placement point were marked on the scalp. Next, a 2.0 cm scalp incision was made to the surface of the skull at each of the marked sites, after which the following steps were performed to implant each skull anchor screw: (1) inserted a 5.5 mm diameter drill guide sleeve into the anchor bracket, (2) drilled to a depth of 5 mm with a 5.1 mm drill bit, (3) replaced the drill guide sleeve and threaded the hole with a machinist's tap and T wrench, (4) screwed nylon skull anchor screws (1/4 inch, 20 threads/inch) into the threaded holes with a driver, (5) removed the driver from the anchor screw and inserted the anchor sleeve through the anchor bracket, twisting to attach it to the skull anchor screw, and (6) inserted the anchor screw through the anchor sleeve and screwed it into the skull anchor screw to secure the frame in place. These steps were repeated for all four screws, progressing from the right posterior to the left

anterior, from the left anterior to the right anterior, and from the right anterior to the left posterior.

MRI acquisition and target planning.

The MRI acquisition protocol was nearly identical to that of the porcine model, however an in-house custom MRI six-channel (rather than four-channel) phased array radio frequency coil (Mayo Clinic, Rochester, MN, USA) was placed on the surface of the head to further enhance the signal to noise ratio. Similar to the *in vivo* pig experiments, COMPASS™ stereotactic surgery planning software was used to identify the stereotactic coordinates of the DBS electrode target and its trajectory path. In conjunction, an in-house extension to 3D Slicer software (J Jacobs, Mayo Clinic, Rochester, MN, USA) which includes visualizations of the MRI data with the stereotactic system was used to assist with the trajectory planning to the thalamic target.

DBS electrode implantation.

The coordinates for the stereotactic device were adjusted to match the thalamic DBS target coordinates and the arc and collar angle values derived during the surgical planning process. DBS electrode implantation was performed identical to that of the porcine experiments with the exception that DBS lead securement was achieved using the Stimloc™ lead anchoring device (Medtronic, Minneapolis, MN, USA).

CT acquisition and electrode confirmation.

The method was identical to that of the porcine experiments.

Results

MRI-compatible stereotactic system design & development

We designed, fabricated, and evaluated a re-attachable stereotactic frame system, based upon the center-of-arc principle and MRI-guidance, to deliver DBS electrodes to anatomical targets defined in stereotactic space (X, Y, Z) with an adjustable trajectory (collar, arc) (figure 2(A)). For stereotactic MRI guidance, we created an N-bar localization system that attaches to the four MRI-compatible implanted screws. Likewise, we created a re-attachable CT localization system to use for DBS electrode localization. The frame system attaches to a stereotactic center calibration device used to validate the mechanical scales of the 3D slide (figure 2(A)). To achieve sub-millimeter mechanical accuracy, the system includes Vernier scales with a resolution of 0.1 mm on the slides used to adjust the 3D Cartesian coordinates (figure 2(B)). The arc and collar are adjustable to the nearest ±1°. The work envelope of the stereotactic system is a 60 × 60 × 90 mm volume that encompasses the cranial cavity; thus, the focus of the arc quadrant system is capable of targeting deep brain regions of interest. Although the trajectories are limited to entry points located on the caudal surface of the skull, the excursion of the trajectory is sufficient for large animal and human DBS surgical procedures.

A key component of this system is the MRI-compatible low-profile self-tapping skull anchor screws, which are implanted to a depth of 5 mm and lie flush with the skull surface

throughout the detachment and re-attachment of the stereotactic devices (figure 2(C)). The base of the head frame system weighs 0.45 kg and attaches directly to the skull anchor screws. The complete stereotactic head frame system weighs 2.00 kg, which is less than the conventional Leksell head frame system which weights 2.27 kg. The entire weight of the system is supported by the skull and does not apply additional torque on the implanted anchor screws. We established a repeatable surgical procedure that utilizes a template to precisely implant the four skull anchor screws (figures 2(D)and (E)). The overall accuracy, repeatability and stability of our re-attachable stereotactic system were validated through phantom, *in vivo* pig, and human cadaver testing.

Repeatability and accuracy validation: phantom testing

Our stereotactic frame system attaches to our custom MRI-compatible phantom (figure 3(A)). The mechanical accuracy was evaluated by adjusting the stereotactic frame system to target each of the nine phantom points (figures 3(B) and 4(A)). To demonstrate repeatability, three independent users repeated frame-based targeting across three separate trials. The root mean square error (RMSE) between the ground truth and the frame-targeted coordinates were calculated across all of the phantom points per user as follows: 0.81 mm, 1.20 mm, and 0.80 mm. Furthermore, to evaluate image accuracy and demonstrate repeatability, a series of four CT and four MR images with the N-bar localization system attached to the phantom were acquired (figure 3(C)). COMPASS™ stereotactic surgery planning software was used to target each phantom point in image space and provide stereotactic coordinates (figures 3(D), (E) and 4(B)). The RMSE between the ground truth and the CT- and MRI-targeted coordinates was calculated across all of the phantom points as 1.11 ±0.40 mm and 1.33 ± 0.38 mm, respectively. Compared to frame-based targeting, CT- and MRI-targeting introduced a maximum RMSE image error of 0.34 and 0.54 mm, respectively. Although the MRI images provide higher resolution views than the CT images, the increased image error is likely due to geometric distortions. For visualization purposes, the ground truth locations of the nine phantom points are plotted in 3D stereotactic space, with the average frame-targeted, CT-targeted, and MRI-targeted coordinates (figures 4(C), 5(A) and (B)).

Stability and accuracy validation: in vivo testing

A mock-human porcine MRI-guided DBS surgical procedure was performed during three independent *in vivo* pig experiments. Figure 6(A) demonstrates the placement of the localizer bracket attached to the four implanted screws with the MRI RF coil in place. Figure 6(B) demonstrates the MRI N-bar localizer box affixed to the localizer bracket prior to the placement of the pig in the MRI. Figures 6(C) and (D) demonstrate the sagittal and coronal MP-RAGE images displayed within the COMPASS™ software, showing the planned target and trajectory used for our final pig experiment. Figure 7(A) demonstrates the experimental setup with the DBS electrode implanted into the target prior to securing the lead to the skull. The focus of our initial *in vivo* pig experiment was the assessment of the mechanics of the surgical procedure and the overall stability of the re-attachable stereotactic frame system. During this first experiment, after a few minor refinements to the surgical procedure, the skull anchor screws were successfully implanted and demonstrated biomechanical stability throughout the remainder of the DBS procedure where the stereotactic devices were detached and re-attached. During the initial experiment, we discovered that it was not

necessary to use a tap to create screw threads to securely implant the skull anchor screws. Further surgical procedure refinement included fabricating guideposts that attach to the implanted anchor screws during placement of the stereotactic devices (N-bar localizer bracket, stereotactic head frame) onto the skull anchor screws. During the second experiment using the refined procedure, the skull anchor screws were securely implanted within ten minutes, and the system exhibited biomechanical stability throughout the DBS procedure. However, it was discovered that the cannula used to implant the DBS electrode was slightly bent, and likely contributed to a calculated 3.52 mm Euclidean distance between the DBS electrode and the planned target. The final *in vivo* pig experiments were primarily focused on accuracy validation. Figure 7(B) shows the pre-surgical plan overlaid onto a post-operative CT, demonstrating the accurate placement of the DBS electrode to planned target. *In vivo* pig testing achieved a 3D Euclidean localization error of 1.70 ± 0.25 mm ($n = 3$, $p < 0.04$) between the pre-operative MRI-planned coordinate and the post-operative CT-confirmed DBS electrode coordinate.

Stability and accuracy validation: cadaver testing

A human cadaver model was used in an MRI-guided DBS surgical procedure during a single experiment to validate translation of the re-attachable porcine stereotactic frame for human-use. Figure 8(A) demonstrates the placement of the modified frame base that was used to guide the implantation of the skull anchor screws. Each of the four anchor screws were implanted into the skull as demonstrated in figure 8(B). Figure 8(C) demonstrates the MRI RF coil in-place on the surface of the head, with the N-bar localizer box attached to the base of the stereotactic frame system. Figure 8(D) demonstrates a coronal view of the pre-operative MRI volume with visible fiducial markers from the N-bar localizer box. Figure 8(E) demonstrates a sagittal view of the pre-operative MRI volume displayed within COMPASS™ software, with the planned DBS electrode trajectory to the thalamic target. The stereotactic plan was also confirmed using Mayo's 3D Slicer Extension software. Figure 9(A) demonstrates the experimental setup used to implant the DBS electrode based on the stereotactic coordinates of the target and trajectory path. The electrode was implanted and secured on the skull with the Stimloc™ system (figure 9(B)). A post-operative CT scan was acquired and used with Mayo's 3D Slicer Extension to assess the accuracy of the DBS lead placement. Figures 9(C)and (D) demonstrate sagittal views of the aligned pre- and post-operative MRI and CT scans with the MRI-based planned DBS electrode target and trajectory overlaid. The calculated 3D Euclidean distance of the implanted electrode to the planned target was within 2.3 mm.

Discussion

Here, we described the successful development of our novel re-attachable stereotactic frame system that includes high-field MRI-compatible anchoring skull screws, MRI and CT stereotactic localization systems, and a stereotactic delivery apparatus comprised of a 3D slide and an adjustable arc-quadrant for stereotactic neurosurgical procedures. We achieved submillimeter mechanical accuracy and demonstrated consistent accuracy across independent phantom tests. Furthermore, using CT- and MRI-guidance to target the phantom points, our system achieved an accuracy that was comparable to a similar experiment which

used MRI-guidance with a Leksell™ stereotactic frame system and reported a Euclidean error of 1.53 mm (Walton *et al* 1996, Owen and Linskey 2009). Further, using a mock-human swine DBS model, we confirmed the accuracy, reliability, and safety of our new re-attachable stereotactic system. After fine-tuning our mock-human surgical procedure, we achieved a 3D Euclidean localization error of 1.70 ± 0.25 mm ($n = 1$, $p < 0.04$) which is comparable to the reported range of average localization errors (1.4 to 2.0 mm) for frame-based clinical DBS procedures (Owen and Linskey 2009). Finally, we translated our results to the human model by demonstrating the stereotactic system's validity in a human cadaver and achieved a 3D Euclidean localization error of 2.3 mm. As such, our *in vivo* and cadaver testing achieved a combined 3D Euclidean localization error of 1.85 ± 0.36 mm ($n = 4$, $p < 0.03$).

As an alternative to frame-based stereotactic systems, frameless technologies continue to emerge, although there is debate regarding their ease-of-use and accuracy compared to conventional stereotactic frame-based approaches (Machado *et al* 2006, Starr *et al* 2010, Mirzadeh *et al* 2014, Chabardes *et al* 2015, Ostrem *et al* 2016). One such system is the Nexframe™ stereotactic system, which uses implanted skull fiducials and leverages intraoperative neuroimaging technologies to achieve 3D spatial accuracy comparable to conventional frame-based approaches (Bot *et al* 2015). In a study comprised of 116 Leksell™ frame-based and seventy-eight Nexframe™ frameless-based DBS electrode implantations, a mean error of 2.5 ± 1.2 mm and 2.8 ± 1.3 mm was reported, respectively (Bot *et al* 2015). Likewise, the Surgical Targeting Fixture (STarFix) microTargeting™ platform (FHC Inc., Bowdoin, Me., USA), considered a frameless stereotactic system due to preplanned trajectories that are custom built, reported comparable accuracy to frame-based systems with an average localization error of 1.99 ± 0.92 mm across seventy-five STarFix-based DBS electrode implantations (Fitzpatrick 2010, Konrad *et al* 2011). This system however is not reusable and intraoperative adjustments are limited. In contrast, our re-attachable stereotactic system is reusable and enables a variety of intraoperative adjustments, maintaining the accuracy and ease-of-use of conventional stereotactic frame-based approaches.

Although the concept of a re-attachable stereotactic frame system dates back decades, our system is the first to demonstrate accurate relocation of stereotactic frame devices during an *in vivo* MRI-guided DBS surgical procedure (Walton *et al* 2000). Over the past decade, DBS therapy has emerged as the standard FDA-approved treatment option to treat medically-refractory movement and mood disruptions associated with Parkinson's disease, essential tremor, dystonia, and obsessive-compulsive disorder (Edwards *et al* 2017). Furthermore, DBS therapy is under investigation for other neurologic and psychiatric disorders, including chronic pain, Tourette's syndrome, Alzheimer's disease, treatment-resistant depression, and addiction (Edwards *et al* 2017). Even so, although an unprecedented number of people have undergone DBS surgery, it remains vastly underutilized compared to the population of patients who would greatly benefit from DBS therapy (Shen 2014). Many good candidates choose not to undergo DBS surgery for various reasons including the risks and costs associated with brain surgery, as well as the fear of being awake with an uncomfortable frame apparatus attached to their head throughout the lengthy surgical procedure. Our stereotactic frame system demonstrates the feasibility of a re-attachable frame-based

stereotactic system that enables the detachment after the surgical planning stage and accurate re-attachment for the electrode implantation stage. Furthermore, the overall weight of our system is less than conventional frame-based Leksell™ stereotactic system. As such, adapting this re-attachable stereotactic platform for clinical use is expected to provide greater patient comfort and decrease time in the operating room given that MR imaging and stereotactic planning can be separated from the surgical procedure requiring the operating room.

In addition, an important aspect of our re-attachable stereotactic frame system is that it enables more complex and chronic neuromodulation experiments in mock-human large animal models of DBS (Min *et al* 2012, Knight *et al* 2013, Paek *et al* 2015, Gibson *et al* 2016, Settell *et al* 2017). Such studies are critical for a better understanding of the latent therapeutic mechanisms of DBS therapies, for investigating chronic DBS-induced neuroplasticity, and for discovering feedback mechanisms to optimize therapy in closed-loop designed DBS systems.

Finally, an innovative aspect of our stereotactic system is that the skull anchor screws are MRI compatible and do not produce imaging artifacts. As such, this system is expected to enable direct targeting for stereotactic neuronavigation by leveraging ultra-high-field (e.g. 7 Tesla) MRI technologies, which provide a high-resolution view of intracranial structures with minimal imaging distortion. This will enable more precise targeting and trajectory planning to mitigate the risks associated with stereotactic neurosurgery and achieve better clinical outcomes. Other stereotactic frames do not meet the safety measures for ultra-high-field MRI system and must use 1.5 T or 3.0 T MR image volumes, where the deep intracranial stereotactic targets are often not clearly visible and require indirect targeting methods. In conclusion, our novel re-attachable stereotactic frame system provides an exciting alternative that is expected to facilitate more sophisticated mock-human DBS studies and clinically advance the field towards more precise personalized neuromodulation therapies to treat a myriad of neurologic and psychiatric disorders.

Acknowledgments

This work was supported by The Grainger Foundation. We thank Terry Reed and the Mayo Clinic Division of Engineering for their hardware fabrication support; Jill Anderson, Andrea McConico, and Bruce Knudsen for their technical support and animal monitoring; Juan Rojas Cabrera and Benjamin Gifford for their support during the studies; Peter Grahn for guidance regarding phantom data analysis and visualizations. Bruce Kall for his stereotactic software technical support; and the Mayo Clinic Center for Advanced Imaging Research for their support.

References

Benabid A L, Pollak P, Louveau A, Henry S and de Rougemont J 1987 Combined (thalamotomy and stimulation) stereotactic surgery of the VIM thalamic nucleus for bilateral Parkinson disease Appl. Neurophysiol 50 344–6 [PubMed: 3329873]

Bot M, van den Munckhof P, Bakay R, Sierens D, Stebbins G and Verhagen Metman L 2015 Analysis of stereotactic accuracy in patients undergoing deep brain stimulation using nexframe and the leksell frame *Stereotact. Funct. Neurosurg.* 93 316–25

Chabardes S et al. 2015 Surgical implantation of STN-DBS leads using intraoperative MRI guidance: technique accuracy and clinical benefit at 1-year follow-up Acta Neurochir. 157 729–37 [PubMed: 25788414]

Edwards C A, Kouzani A, Lee K H and Ross E K 2017 Neurostimulation devices for the treatment of neurologic disorders Mayo Clin. Proc 92 1427–44 [PubMed: 28870357]

Fedorov A et al. 2012 3D Slicer as an image computing platform for the quantitative imaging network Magn. Reson. Imaging 30 1323–41 [PubMed: 22770690]

Felix B, Leger M E, Albe-Fessard D, Marcilloux J C, Rampin O and Laplace J P 1999 Stereotaxic atlas of the pig brain Brain Res. Bull 49 1–137

Fitzpatrick J M 2010 The role of registration in accurate surgical guidance Proc. Inst. Mech. Eng. H 224 607–22 [PubMed: 20718266]

Gibson W S, Ross E K, Han S R, Van Gompel J J, Min H K and Lee K H 2016 Anterior thalamic deep brain stimulation: functional activation patterns in a large animal model Brain Stimul. 9 770–3 [PubMed: 27160467]

Goerss S, Kelly P J, Kall B and Alker G J, Jr 1982 A computed tomographic stereotactic adaptation system Neurosurgery 10 375–9 [PubMed: 7041006]

Grahn P J et al. 2016 MRI-guided stereotactic system for delivery of intraspinal microstimulation Spine 41 E806–13 [PubMed: 26679880]

Kelly P J, Sharbrough F W, Kall B A and Goerss S J 1987 Magnetic resonance imaging-based computer-assisted stereotactic resection of the hippocampus and amygdala in patients with temporal lobe epilepsy Mayo Clin. Proc 62 103–8 [PubMed: 3543519]

Knight E J. Nucleus accumbens deep brain stimulation results in insula and prefrontal activation: a large animal FMRI study. PLoS One. 2013; 8:e56640. [PubMed: 23441210]

Konrad P E et al. 2011 Customized, miniature rapid-prototype stereotactic frames for use in deep brain stimulator surgery: initial clinical methodology and experience from 263 patients from 2002 to 2008 Stereotact. Funct. Neurosurg. 89 34–41

Machado A, Rezai A R, Kopell B H, Gross R E, Sharan A D and Benabid A L 2006 Deep brain stimulation for Parkinson's disease: surgical technique and perioperative management Mov. Disord 21 S247–58 [PubMed: 16810722]

Min H K et al. 2012 Deep brain stimulation induces BOLD activation in motor and non-motor networks: an fMRI comparison study of STN and EN/GPi DBS in large animals NeuroImage 63 1408–20 [PubMed: 22967832]

Min H K et al. 2014 Subthalamic nucleus deep brain stimulation induces motor network BOLD activation: use of a high precision MRI guided stereotactic system for nonhuman primates Brain Stimul. 7 603–7 [PubMed: 24933029]

Mirzadeh Z, Chapple K, Lambert M, Dhall R and Ponce F A 2014 Validation of CT-MRI fusion for intraoperative assessment of stereotactic accuracy in DBS surgery Mov. Disord 29 1788–95 [PubMed: 25377213]

Nakazawa H et al. 2014 Geometric accuracy of 3D coordinates of the Leksell stereotactic skull frame in 1.5 Tesla- and 3.0 Tesla-magnetic resonance imaging: a comparison of three different fixation screw materials J. Radiat. Res. 55 1184–91 [PubMed: 25034732]

Neumann J O, Giese H, Biller A, Nagel A M and Kiening K 2015 Spatial distortion in MRI-guided stereotactic procedures: evaluation in 1.5-, 3- and 7 Tesla MRI scanners Stereotact. Funct. Neurosurg 93 380–6

Ostrem J L et al. 2016 Clinical outcomes using ClearPoint interventional MRI for deep brain stimulation lead placement in Parkinson's disease J. Neurosurg 124 908–16 [PubMed: 26495947]

Owen C M and Linskey M E 2009 Frame-based stereotaxy in a frameless era: current capabilities, relative role, and the positive- and negative predictive values of blood through the needle J. Neurooncol. 93 139–49 [PubMed: 19430891]

Paek S B et al. 2015 Frequency-dependent functional neuromodulatory effects on the motor network by ventral lateral thalamic deep brain stimulation in swine NeuroImage 105 181–8 [PubMed: 25451479]

Picard C, Olivier A and Bertrand G 1983 The first human stereotaxic apparatus. The contribution of Aubrey Mussen to the field of stereotaxis J. Neurosurg. 59 673–6 [PubMed: 6350539]

Seibert T M et al. 2016 Distortion inherent to magnetic resonance imaging can lead to geometric miss in radiosurgery planning Pract. Radiat. Oncol 6 e319–28 [PubMed: 27523440]

Settell M L et al. 2017 Functional circuitry effect of ventral tegmental area deep brain stimulation: imaging and neurochemical evidence of mesocortical and mesolimbic pathway modulation Frontiers Neurosci. 11 104

Shen H 2014 Neuroscience: tuning the brain Nature 507 290–2 [PubMed: 24646978]

Sironi V A 2011 Origin and evolution of deep brain stimulation *Frontiers Integr.* Neurosci. 5 42

Spiegel E A and Wycis H T 1952 Stereoencephalotomy (Thalamotomy and Related Procedures). Part I —Methods and Stereotaxic Atlas of the Human Brain (New York: Grune & Stratton)

Spiegel E A, Wycis H T, Marks M and Lee A J 1947 Stereotaxic apparatus for operations on the human brain Science 106 349–50 [PubMed: 17777432]

Starr P A, Martin A J, Ostrem J L, Talke P, Levesque N and Larson P S 2010 Subthalamic nucleus deep brain stimulator placement using high-field interventional magnetic resonance imaging and a skull-mounted aiming device: technique and application accuracy J. Neurosurg 112 479–90 [PubMed: 19681683]

Walton L et al. 2000 Development of a relocatable frame technique for gamma knife radiosurgery. Technical note *J. Neurosurg.* 93 198–202 (PMID:) [PubMed: 11143248]

Walton L, Hampshire A, Forster D M and Kemeny A A 1996 A phantom study to assess the accuracy of stereotactic localization using T1-weighted magnetic resonance imaging with the Leksell stereotactic system Neurosurgery 38 170–6 (discussion 176–8) [PubMed: 8747966]

Wang D D, Lau D, Rolston J D, Englot D J, Sneed P K and McDermott M W 2014 Pain experience using conventional versus angled anterior posts during stereotactic head frame placement for radiosurgery J. Clin. Neurosci 21 1538–42 [PubMed: 24814855]

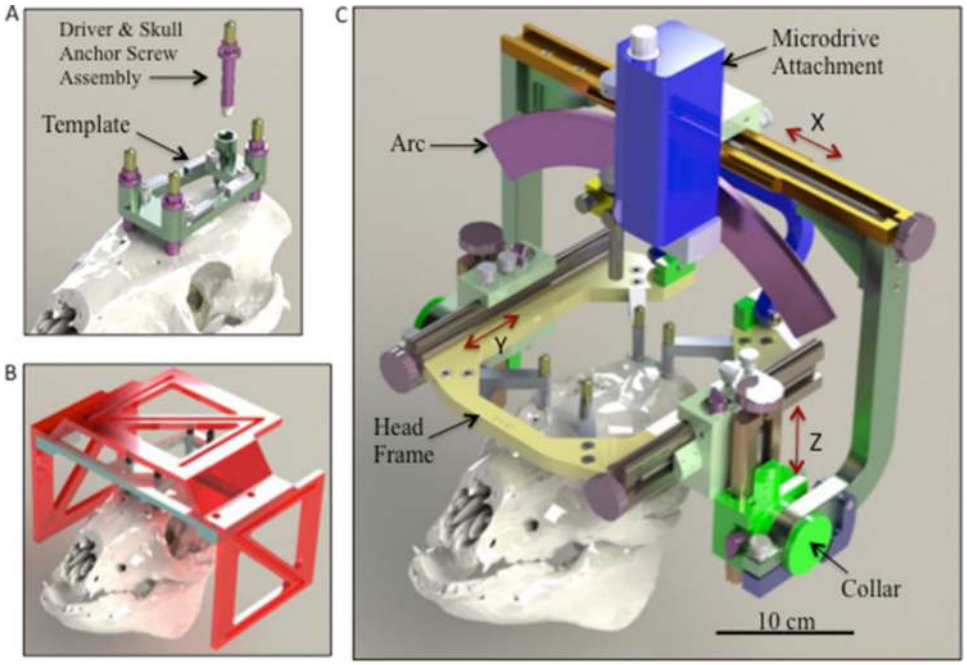

Figure 1.

(A) Skull anchor screw template and driver assembly to guide implantation of four MRI-compatible PEEK anchor skull screws. (B) MRI-compatible acrylic N-bar localizer box affixed to the MRI-compatible acrylic bracket, attached to four PEEK anchor skull screws via DuPont™ Delrin® plastic screws. (C) Stereotactic arc-centered system affixed to the base of the head frame, which is attached to four skull anchor screws.

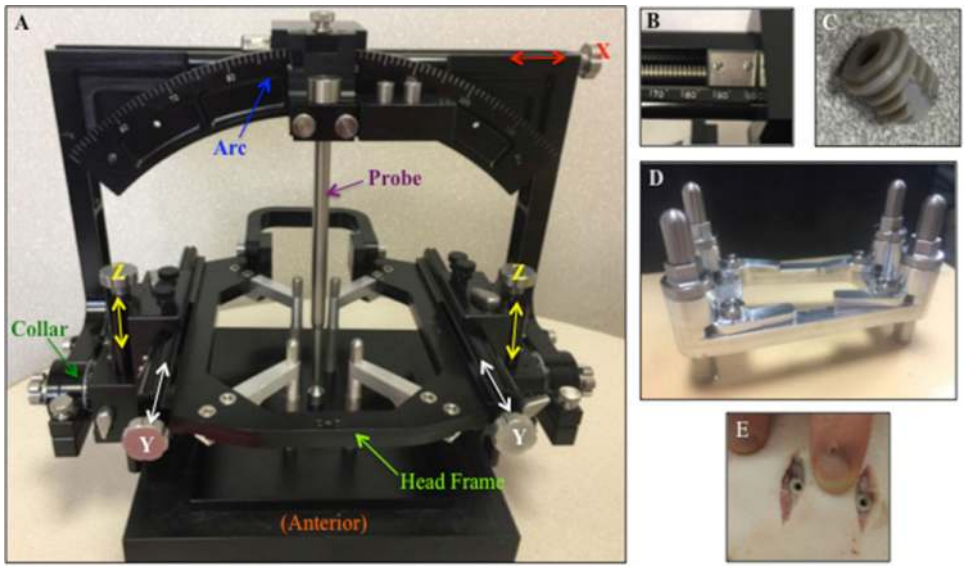

Figure 2.

(A) Stereotactic frame system attached to arc center calibration device. (B) Vernier scale on *x*-axis. (C) Skull anchor screw. (D) Skull anchor screw template. (E) Implanted anchor screws.

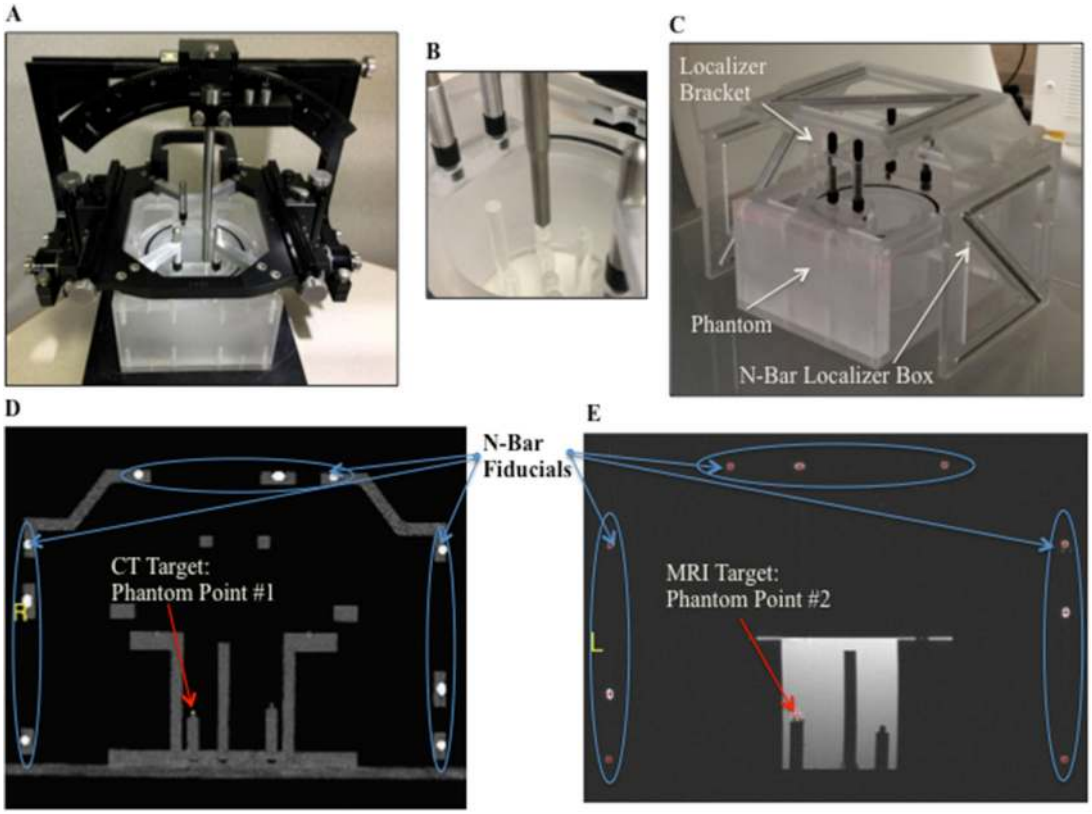

Figure 3.

(A) Stereotactic frame system attached to phantom. (B) Zoomed in view of mechanical targeting phantom point #2. (C) N-Bar CT localizer box attached to phantom within the CT scanner core. (D) Coronal view of CT scan with phantom point #1 targeted. (E) Coronal view of MRI scan of phantom point #4 targeted.

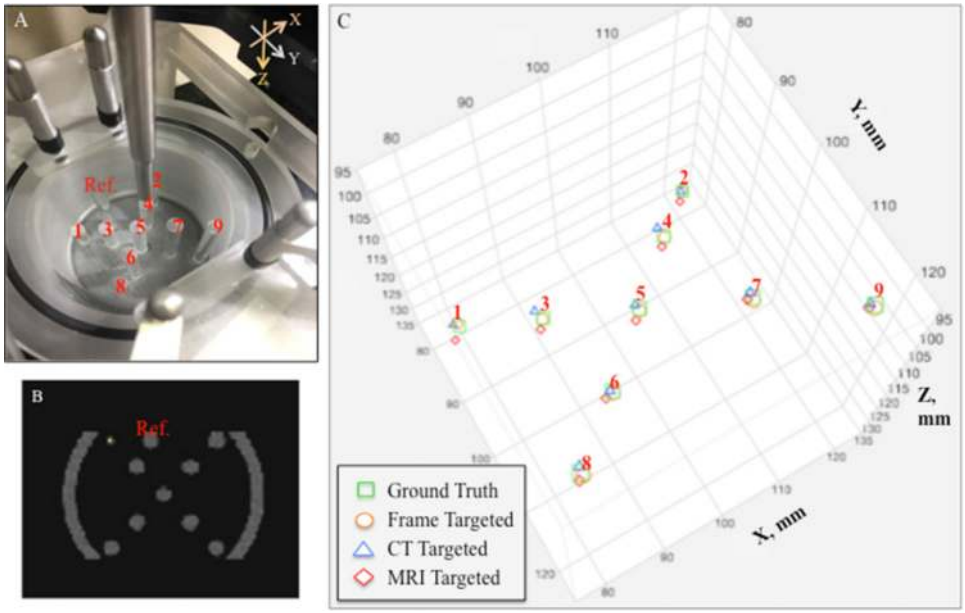

Figure 4.

(A) Phantom with points 1 through 9 and the reference point labeled. (B) Axial view of CT scan of phantom with the reference point labeled and phantom point #1 targeted. (C) Plot of the actual and targeted stereotactic coordinates for each phantom point.

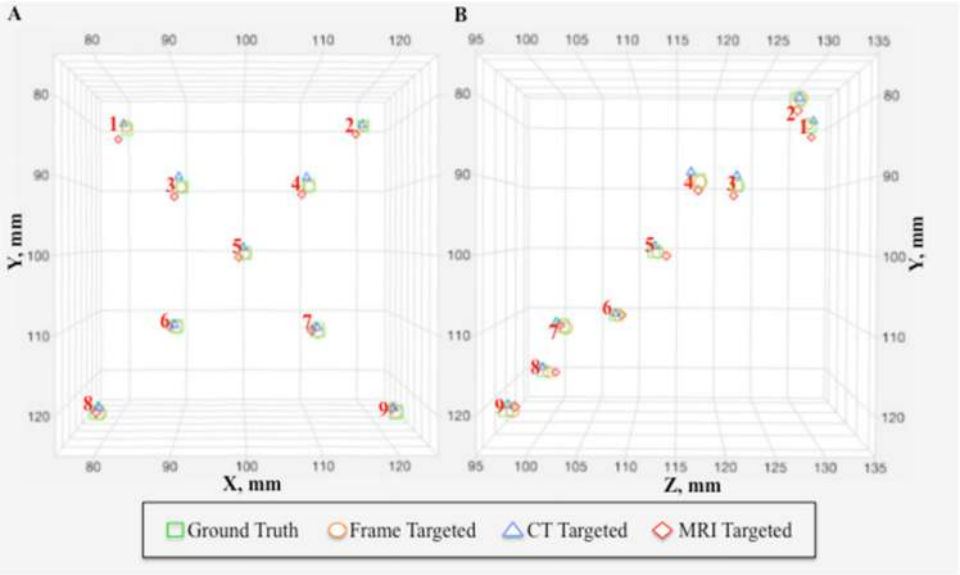

Figure 5.
(A) and (B) Multiple orientations of the ground truth locations of the nine phantom points plotted in 3D stereotactic space with the average frame-targeted, CT-targeted, and MRI-targeted coordinates.

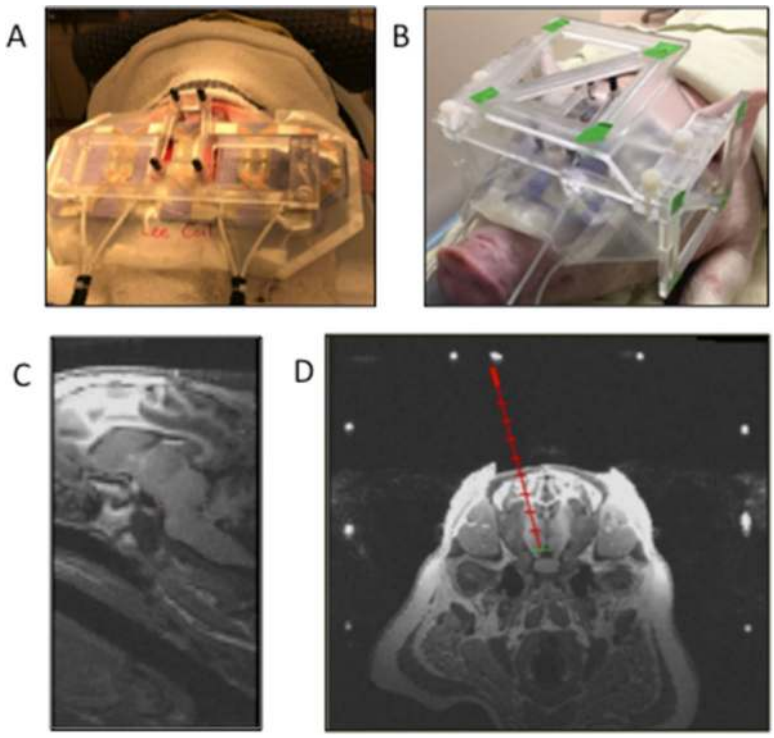

Figure 6.

(A) MRI RF coil and N-bar localizer bracket attached to implanted anchor skull screws. (B) MRI N-bar localizer box attached to bracket. (C) Sagittal view of MRI stereotactic target. (D) Coronal view of MRI stereotactic planning of DBS electrode trajectory and targeting (red line).

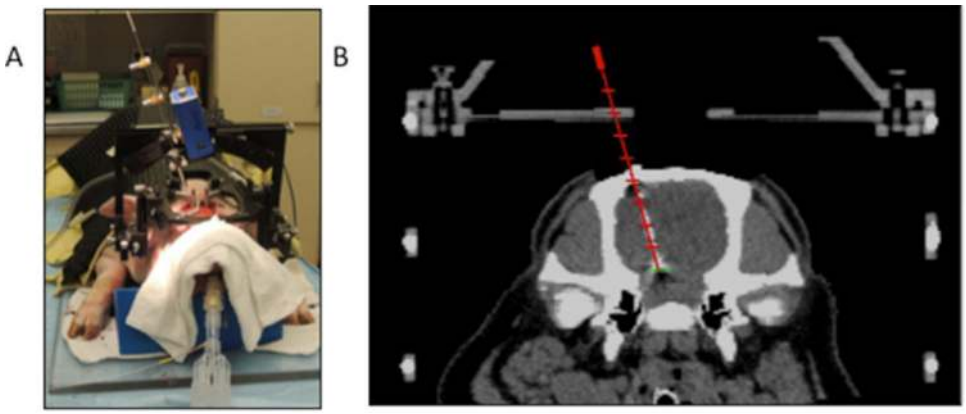

Figure 7.
(A) Experimental setup to implant DBS electrode using the stereotactic frame system. (B) Post-operative CT with overlay of pre-operative MRI planned target and electrode trajectory (red line).

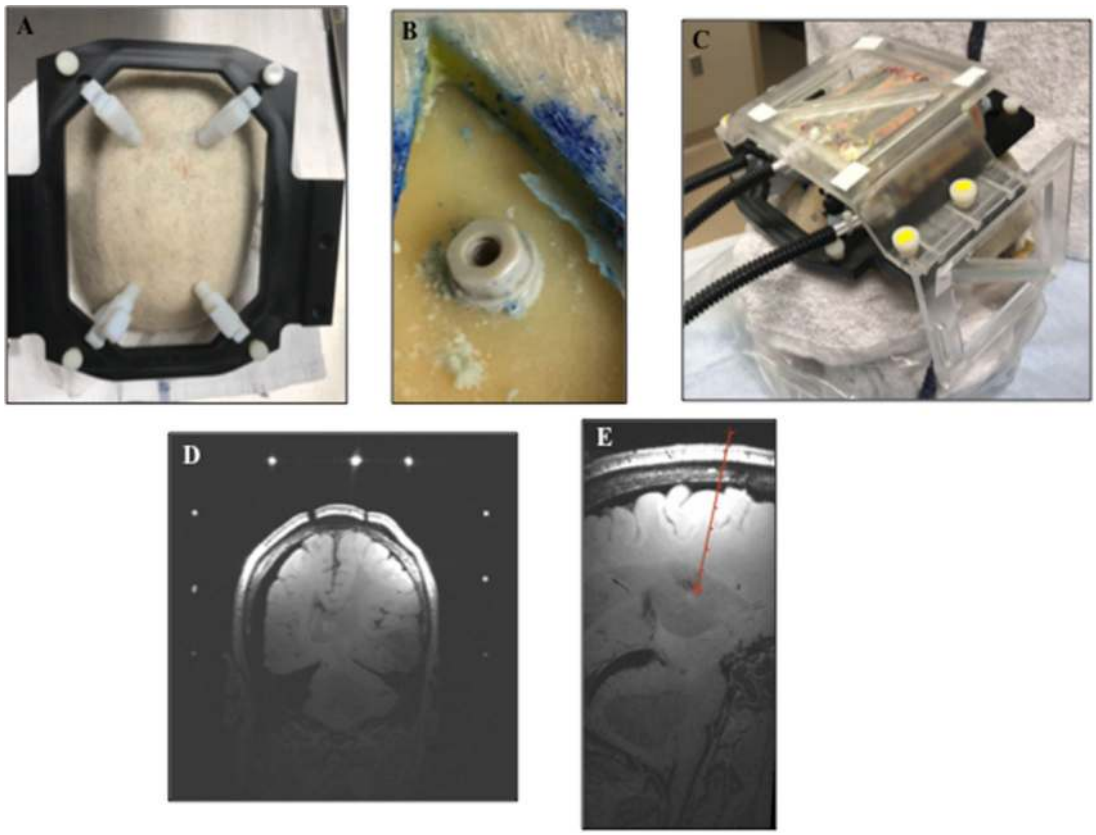

Figure 8.

(A) Modified frame base used as a template to implant the screws and to attach stereotactic devices to the implanted screws. (B) Implanted skull anchor screw. (C) MRI RF coil on the surface of the skull with the N-bar localizer box attached to the frame base, which is attached to the skull anchor screws. (D) Coronal view of a pre-operative MRI scan with visible N-bar fiducial markers. (E) Sagittal view of MRI stereotactic planning of DBS with electrode trajectory and target point (red line).

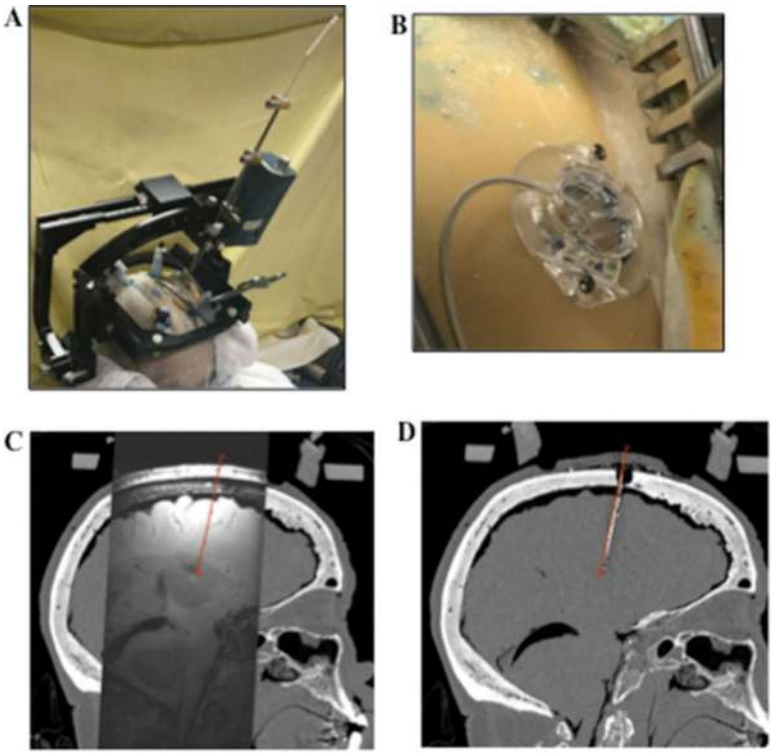

Figure 9.

(A) Experimental setup to implant a DBS electrode using the stereotactic frame system. (B) Implanted electrode with Stimloc™ in place. (C) and (D) Sagittal views of the pre- and post-operative MRI and CT scans aligned and the MRI-based planned DBS electrode target and trajectory (red line) overlaid onto the postoperative CT scan.